

# Exact Solutions for Solitary Waves in a Bose-Einstein Condensate under the Action of a Four-color Optical Lattice

Barun Halder<sup>1</sup>, Suranjana Ghosh<sup>2</sup>, Pradosh Basu<sup>1</sup>, Jayanta Bera<sup>1</sup>, Boris Malomed<sup>3,4</sup>, and Utpal Roy<sup>1</sup>

<sup>1</sup>*Indian Institute of Technology Patna, Bihta, Patna-801103, India*

<sup>2</sup>*Indian Institute of Science Education and Research Kolkata, Mohanpur-741246, India*

<sup>3</sup>*Department of Physical Electronics, School of Electrical Engineering, Faculty of Engineering, and Center for Light-Matter Interaction, Tel Aviv University, P.O.B. 39040, Ramat Aviv, Tel Aviv, Israel*

<sup>4</sup>*Instituto de Alta Investigación, Universidad de Tarapacá, Casilla 7D, Arica, Chile*

We address dynamics of Bose-Einstein condensates (BECs) loaded into a one-dimensional four-color optical lattice (FOL) potential with commensurate wavelengths and tunable intensities. The analysis identifies specific multi-parameters forms of the FOL potential which admits exact solitary-wave solutions. This newly found class of potentials includes more particular species, such as frustrated double-well superlattices and bichromatic and three-color lattices. Our exact solutions provide options for controllable positioning of density maxima of the localized patterns, and tunable Anderson-like localization in the frustrated potential. A numerical analysis is performed to establish dynamical stability and structural stability of the obtained solutions, which makes them relevant for experimental realization. The newly found solutions offer applications to the design of schemes for quantum simulations and processing quantum information.

PACS numbers: .....

## I. INTRODUCTION

A suitably prepared standing wave of laser radiation can form an optical lattice (OL), which are broadly used for trapping and steering of ultracold atoms [1–8]. Offering a versatile platform for research in the area of matter waves, OLs have become the most appropriate candidate for the realization of quantum simulations [9–11]. Further, ultracold atoms and Bose-Einstein condensates (BECs) trapped in an OL are used as a basis for the development of atomic clocks, quantum sensors, quantum computers, and a variety of other applications in quantum technologies [12–14].

In particular, the study of BEC under the action of geometrically frustrated OLs has drawn much interest [15–18]. Many complex phenomena have been found in this connection, including Anderson-like localization and negative absolute temperature [17, 19–21]. Optical superlattices subjected to frustration offer a potential for the development of tools which can hold and mould robust matter-wave states, such as solitons [22–26]. Theoretical studies in this direction are chiefly limited to a variety of bi-color optical lattices (BOL). A more general form of multi-color OLs may offer additional advantages, including the following points: (i) the color (wavelength) and intensity of the constituent beams, building the effective optical potential, greatly influence the manner in which the atoms are trapped; (ii) the formation of solitons requires a specific correlation between the nonlinearity and the trap parameters, which the multi-color OL may help to maintain; (iii) relations between intensities of the constituent beams may be used to optimize the creation of the self-trapped patterns. Thus, multi-color beams can be used to design potentials necessary for holding complex soliton patterns.

The aim of this work is to introduce a four-color OL (FOL) with commensurate wavelengths, which acts on a cigar-shaped (quasi-one-dimensional) BEC with the cubic nonlinearity. The corresponding Gross-Pitaevskii equation (GPE) is used to find appropriate relations between the nonlinearity and the potential parameters which help to support solitons. We produce analytical solutions which identify the specific form of the FOL and its parameter domain which provide tunability of the soliton-building scheme. Many exact condensate wave functions are obtained, and the results are illustrated by several characteristic examples. These solutions may be used for applications similar to those proposed in previous works [27–32]. Stability of the exact wave functions is addressed by means of direct simulations, adding random perturbations either to the underlying stationary solution, or to the external trap (the latter implies the consideration of the structural stability of the exact solutions). We thus find that our solutions are fully stable, both dynamically and structurally.

## II. EXACT ANALYTICAL MODEL FOR OBTAINING THE SOLITARY EXCITATIONS UNDER THE NOVEL FOL TRAP

The FOL potential is produced by the combinations of four OLs with commensurate wave numbers,  $l$ ,  $2l$ ,  $3l$ , and  $4l$ , while the corresponding intensities of the laser beams,  $V_{1,2,3,4}$ , are treated as free parameters, with the intention to find appropriate relations between them. The corresponding effective potential acting on atoms is

$$V(z) = \sum_{j=1}^4 V_j \cos(jlz). \quad (1)$$

The lattice depth may be compared to the recoil energy,  $E_R = 2\pi^2\hbar^2/(M\lambda^2)$ , and the scaled lattice wave-vector is given by  $l = 2\pi a_\perp/\lambda$ , where  $\lambda$  is the wavelength,  $M$  is the mass of the BEC atom,  $a_\perp = (\hbar/(M\omega_\perp))^{1/2}$  and  $\omega_\perp$  is the transverse frequency. The dimensionless 1D-GPE has the form

$$\left[ i \frac{\partial}{\partial t} + \frac{1}{2} \frac{\partial^2}{\partial z^2} - g(z, t) |\psi(z, t)|^2 - V(z) - i\tau(z, t) \right] \psi(z, t) = 0. \quad (2)$$

Here,  $g(z, t)$  is the nonlinearity coefficient, which may be made space- and time-modulated, while  $\tau(z, t)$  represents the space- and time-modulated loss or gain of the condensate atoms. For illustration, we have exploited experimentally feasible parameters of Li<sup>7</sup> BEC in the quasi-1D trapping configuration with transverse frequency  $\omega_\perp = 2\pi \times 710$  Hz, OL wavelength  $\lambda = 10.62$   $\mu\text{m}$ , and scattering length  $a_s = -0.21$  nm corresponding to attractive interactions between atoms [33]. By varying the applied magnetic field and angle between the overlapping laser beams, it is possible to engineer the shape of the external potential [34, 35].

To produce a spatially localized solution of Eq. (2), following the general scheme used for engineering matter-wave configurations [36, 37] we choose an ansatz,

$$\psi(z, t) = A(z, t) F(B(z, t)) e^{i\theta(z, t)}, \quad (3)$$

such that the external potential is supposed to be precisely found by exactly solving  $B(z, t)$ , amplitude  $A(z, t)$ , phase  $\theta(z, t)$  and the condensate form factor  $F[B(z, t)]$ . We substitute this ansatz into the GPE (2) and separate out the real and imaginary parts. To establish relations between the physically relevant quantities like nonlinearity, amplitude, phase and external trap for a solitary wave solution, the real part can be mapped to the following nonlinear differential equation,

$$\frac{\partial^2 F[B(z, t)]}{\partial B(z, t)^2} - GF^3[B(z, t)] = 0, \quad (4)$$

which introduces a constant  $G = 2g(z, t)A^2(z, t)/B_z^2(z, t)$  in the case of solitary wave excitations.  $G$  is  $-1$  for attractive and  $1$  for repulsive inter-atomic interactions. The last consistency condition in Eq. (4) is nothing but the elliptic equation, whose exact solutions are well-known in the form of 12 Jacobian elliptic functions ( $cn[z, m]$ ,  $sn[z, m]$  etc), where  $m$  is the modulus parameter with  $0 \leq m \leq 1$  [38]. One can choose various shapes of the elliptic functions from periodic ( $m = 0$ ) to localized ( $m = 1$ ), by varying the value of its modulus parameter. Here, we will emphasize only on the localized forms of the elliptic functions, *i.e.*,  $cn[z, 1] = \text{sech}[z]$ , for the bright soliton case with attractive nonlinearity and

$sn[z, 1] = \tanh[z]$  for the dark soliton case with repulsive nonlinearity. In addition to solving the above mentioned equation, we also obtain the following consistency relations:

$$\begin{aligned} GB_z^2(z, t) - 2A^2(z, t)g(z, t) &= 0, \\ B_t(z, t) + B_z(z, t)\theta_z(z, t) &= 0, [A^2(z, t)B_z(z, t)]_z = 0 \\ 2A(z, t)A_t(z, t) + [A^2(z, t)\theta_z(z, t)]_z \\ &\quad - 2\tau(z, t)A^2(z, t) = 0 \\ \frac{A_{zz}(z, t)}{2A(z, t)} - \frac{\theta_z^2(z, t)}{2} - \theta_t(z, t) - V(z) &= 0 \end{aligned} \quad (5)$$

where the subscripts stand, as usual, for partial derivatives. The above set of equations is solved simultaneously to produce

$$\begin{aligned} B(z, t) &= \frac{c(t)}{A^2(z, t)}, \quad \theta_z(z, t) = -\frac{A_t(z, t)}{A_z(z, t)}, \\ g(z, t) &= GB_z^2(z, t)/2A^2(z, t), \end{aligned} \quad (6)$$

where  $c(t)$  is an arbitrary positive definite function of time. These equations indicate a direct dependence of phase and nonlinearity on the amplitude of the system which will be determined by the trapping potential through the last equation of system (5).

We substitute the expression of the external potential from Eq. (4) into the set of equations (5-6) and obtain the amplitude, phase and nonlinearity in the following exact forms:

$$\begin{aligned} A(z, t) &= \sqrt{\frac{c(t)}{\gamma \exp(b_1 \cos(lz) + b_2 \cos(2lz))}}, \\ \theta(z, t) &= \frac{1}{16}(l^2 b_1^2 + l^2 b_2^2)t, \quad \tau(z, t) = \frac{1}{2} \frac{c'(t)}{c(t)}, \\ g(z, t) &= \frac{G\gamma^4}{2c^2(t)} \exp(4b_1 \cos(lz) + 4b_2 \cos(2lz)). \end{aligned} \quad (7)$$

We have here introduced two real constants,  $b_1$  and  $b_2$ , which help us to define the final form of the FOL-amplitudes:

$$\begin{aligned} V_1 &= (1 + b_2) \frac{l^2 b_1}{4}, \quad V_2 = \left( \frac{-b_1^2}{16} + b_2 \right) l^2, \\ V_3 &= -\frac{l^2 b_1 b_2}{4}, \quad V_4 = -\frac{l^2 b_2^2}{4}. \end{aligned} \quad (8)$$

This is one of the essential results of the present work. Constants  $b_1$  and  $b_2$  are thus identified as the prime tuning parameters for controlling the trapping potential and condensate density. For the attractive and repulsive interactions, assuming the commonly known bright- or dark-soliton solution of the elliptic equation (Eq. (4)), the condensate wave functions take, severally, the following form:

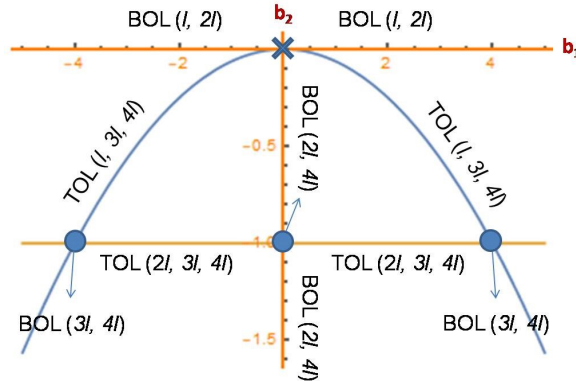


FIG. 1. Curves and points for  $l = 0.84$  where the potential is not a FOL, but a TOL or a BOL. ‘ $\times$ ’ signifies no potential for  $b_1 = b_2 = 0$ . All other points in the  $(b_1, b_2)$  plane correspond to FOLs.

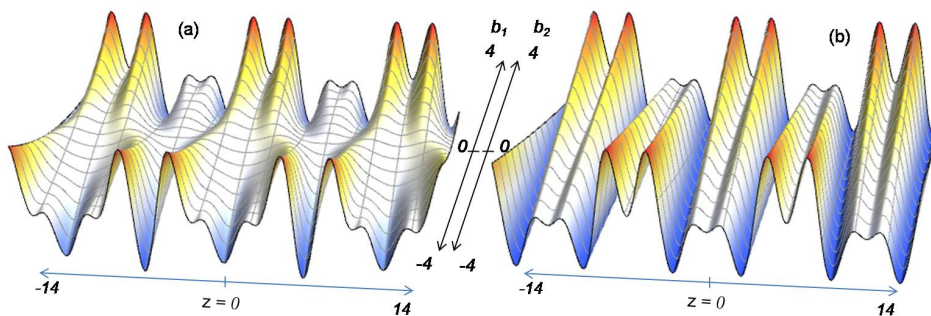


FIG. 2. The variation of the FOL potential following the change of the tuning parameters for  $l = 0.84$ : (a) for fixed  $b_2 = 2$ ,  $b_1$  varies from  $-4$  to  $+4$ ; (b) for fixed  $b_1 = 2$ ,  $b_2$  varies from  $-4$  to  $+4$ . Here and in the figures following below, the results are displayed in interval  $-14 < z < +14$ .

$$\begin{aligned} \psi(z, t) &= \sqrt{\frac{c(t)}{\gamma \exp[b_1 \cos(lz) + b_2 \cos(2lz)]}} \operatorname{sech} \left[ \gamma \int_0^z \exp(b_1 \cos(lz) + b_2 \cos(2lz)) dz' \right] \exp(i\theta(z, t)), \\ \psi(z, t) &= \sqrt{\frac{c(t)}{\gamma \exp(b_1 \cos(lz) + b_2 \cos(2lz))}} \tanh \left[ \gamma \int_0^z \exp(b_1 \cos(lz) + b_2 \cos(2lz)) dz' \right] \exp(i\theta(z, t)) \end{aligned} \quad (9)$$

We are now in a position to analyze the relevant potential profiles and the corresponding condensate densities. Condensate densities will be delineated in Fig. 3 and Fig. 4 for some parameter domains of  $b_1$  and  $b_2$  with  $c = 0.1$ ,  $g = 0.1$ , and  $l = 0.84$ .

### III. THE PARAMETER DOMAIN AND SHAPE OF THE TUNABLE FOL

Figure 1 depicts the structure in the  $(b_1, b_2)$  space, produced by Eq. (8), where one obtains, as particular cases, a tri-color optical lattice (TOL), or a BOL. On the contrary, FOL is obtained in the entire space, excluding the curves and points indicated in the figure.

The respective FOL potential, drawn in Fig. 2, seems

interesting enough. For  $b_1 > 0$  and  $b_2 > 0$ , the FOL is a disordered double-well superlattice, featuring frustrations in terms of both inter- and intra-well separations. Figures 2(a) and (b) reduce to a BOL at  $b_1 = b_2 = 0$ . However, the transition to the domain of  $b_1 < 0$  or  $b_2 < 0$  makes the potential shapes quite different. In the former case, triple-well superlattice gradually appears at  $b_1 < 0$ , whereas in the latter case, a translational shift of the double-wells in the superlattice by half a period is observed. The presently engineered FOL may be the most advanced trapping potential for BEC, derived as an ingredient of exact solutions. It may find applications to the design of quantum simulation, information and computation schemes [28–31]. We will further illustrate the results by displaying density patterns.

#### IV. DENSITY PATTERNS SUPPORTED BY THE ENGINEERED FOL

The density patterns in the domain of  $b_{1,2} > 0$  are displayed in Fig. 3, along with the respective trapping profile, which help to understand the formation mechanism for the patterns. The presence of the inter- and intra-well potential frustration helps one to realize well-distinguished quantum clouds, that may be employed for the design of enhanced atom-interferometry (Fig. 3(a-c)). When the intra-well frustration disappears, the previously separated clouds inside the double well become indistinguishable and the condensate starts accumulating at the central frustrated site, causing Anderson-like localization (Fig. 3(d)). The wide tunability of the FOL and the corresponding mesoscopic clouds make it possible to predict a variety of quantum states, that may be useful for quantum technology [39–41].

In Fig. 4, we illustrate the situation in the negative domain:  $b_1 < 0$  in Fig. 4(a-b),  $b_2 < 0$  in Fig. 4(c), and  $b_{1,2} < 0$  in Fig. 4(d). It produces several aligned well-separated spatial Schrödinger-cat states for  $b_1 < 0$  [42]. More negative  $b_1$  offers localization of the cat-state at the central double well. For  $b_2 < 0$ , the resulting triple-well super-lattice generates an odd number of well-separated clouds. Interestingly, changing the sign of  $b_1$  at  $b_2 < 0$  spatially translates the triple-well lattice by one period to create a single BEC-cloud at the center (Fig. 4(d)). Thus, a transition from Fig. 4(d) to Fig. 4(c) splits the single cloud into a set of three ones. In addition, a transition from Fig. 4(b) to Fig. 4(a) splits the Schrödinger-cat state from one to three. Along with the above-mentioned possibilities, this scheme of potential engineering offers an efficient scheme for designing quantum logic gates [31, 32, 43–46]. To illustrate the temporal dynamics of one of the obtained solutions, we choose the trap corresponding to  $b_1 = 2$  and  $b_2 = 1$  which shows a frustrated double-well super-lattice. Condensate, trapped in this potential, is allowed to evolve in time with a random noise of amplitude 10% of the maximum density. Condensate densities are depicted in Fig. 5(a-c) for  $t = 0$ ,  $t = 10ms$ , and  $t = 20ms$ , respectively. One can observe that the condensate is maintaining its shape after  $t = 10ms$ , but getting distorted at  $t = 20ms$ .

#### V. DYNAMICAL STABILITY AND STRUCTURAL STABILITY OF THE CONDENSATE

It is obviously necessary to check the dynamical and structural stability of the special analytical solution produced above. The dynamical stability pertains to disturbance added to the wave function, while the structural stability implies deformation of the external trap. We addressed these problems separately by numerically solving the GPE with the help of the split-step Fourier method [21, 24, 32]. The results are presented in Fig. 6. In the

former case, we have added random white noise  $\mathfrak{R}_w$  to the analytically obtained wave function, while in the latter case, the noise is added to the external trap. The noisy form of the initial wave function and potential are represented as

$$\begin{aligned}\psi_{\text{noisy}}(z, t = 0) &= \psi(z, t = 0) + \mathfrak{R}_w \\ V_{\text{noisy}}(z) &= V(z) + \mathfrak{R}_w.\end{aligned}\quad (10)$$

While the stability analysis was performed for a broad range of the parameters, here we choose  $b_1 = 2$  and  $b_2 = 1$  for the purpose of illustration. In Fig. 6, the condensate density profile, along with the external trap (not in scale), are depicted without the noise. The wave function is numerically evolved for both the noisy configurations defined as per Eq. 10. Amplitude of noise  $\mathfrak{R}_w$  varies from 0 to 5% of the maximum amplitude of the initial wave function. In the first scenario, we monitored the evolution of the wave functions, induced by the inputs  $\psi_{\text{noisy}}(z, t = 0)$  and  $\psi(z, t = 0)$ , with our model potential,  $V(z)$ . To observe the stability of the stationary state, we computed deviation of the evolving condensate density ( $D_W$ ). In the latter case, we monitored the evolution of the input wave function ( $\psi(z, t = 0)$ ) under the action of the potentials  $V_{\text{noisy}}(z)$  and  $V(z)$ , to observe the structural deformation in the condensate density ( $D_P$ ). We have simulated the evolution for 10000 time iterations with properly chosen space and time steps,  $dz = 0.277 \mu\text{m}$  and  $dt = 0.22 \mu\text{s}$ , respectively. The deviation (maximum relative error) of the evolved noisy data from their noise-free counterparts is shown for both kinds of the stability analyses in Fig. 6 by the upper curve (\*) and lower one,  $\oplus$ . Observing the noisy density profile after 10000 iterations, we conclude that the density patterns retain their shapes with minimal deformation, which implies that the analytical solutions are indeed stable against both kinds of the random perturbations (Fig. 6). The observed relative perturbation in the final configurations is near to 1% when the noise is initially added to the wave function, and near to 2% when it is added to the trapping potential. Thus, the presented model and its analytical solutions are physically relevant ones.

#### VI. CONCLUSION

We have reported the exact form of the FOL (four-color optical lattice) trap for the BEC in one dimension, which makes it possible to produce exact solutions for the trapped condensate. A variety of experimentally relevant trap profiles are reported, including one-, two-, three- and four-color OLs with tunable shapes. It is worthy to stress that there are only two FOL-tuning parameters,  $b_1$  and  $b_2$ , instead of four, making the detailed analysis of the exact solutions feasible. For a chosen trap parameters, the exact condensate density is illustrated and its variations after evolving in time are also shown. By means of systematic simulations, we have established dynamical and structural stability of the exact solutions. The stability

against structural perturbations is especially important, as the solutions are valid only for the specially designed form of the FOL potentials. This class of FOL trapping

potentials offers a straightforward potential for the use in applications, such as quantum simulation and other quantum technologies [13, 28–31, 39–41].

- 
- [1] Bloch I, Dalibard J and Zwirger W 2008 *Rev. Mod. Phys.* **80** 885.
- [2] Greiner M, Mandel O, Esslinger T, Hänsch T W and Bloch I 2002 *Nature* **415** 39.
- [3] Denschlag J H, Simsarian J E, Häffner H, McKenzie C, Browaeys A *et. al.* 2002 *J. Phys. B: At. Mol. Opt. Phys.* **35** 3095.
- [4] Jaksch D, Bruder C, Cirac J I, Gardiner C W and Zoller P 1998 *Phys. Rev. Lett.* **81** 3108.
- [5] Brazhnyi V A and Konotop V V 2004 *Mod. Phys. Lett. B* **18** 627-651.
- [6] Morsch O. and Oberthaler M 2006 *Rev. Mod. Phys* **78** 179-212.
- [7] Lewenstein M, Sanpera A, and Ahufinger V *Ultracold Atoms in Optical Lattices: Simulating Quantum Many-Body Systems* (Oxford: Oxford University Press, 2012).
- [8] Dutta O, Gajda M, Hauke P, Lewenstein N, Luhmann D S, Malomed B, Sowinski T and Zakrzewski J Non-standard Hubbard models in optical lattices: a review, 2015 *Rep. Prog. Phys.* **78**, 066001.
- [9] Hauke P, Cucchiatti F M, Tagliacozzo L, Deutsch I and Lewenstein M 2012 *Rep. Prog. Phys.* **75**, 082401.
- [10] Gross C and Bloch I 2017 *Science* **357** 6355.
- [11] Schäfer F, Fukuhara T, Sugawa S, Takasu Y and Takahashi Y 2020 *Nat. Rev. Phys.* **2** 411.
- [12] Brennen G K, Pupillo G, Rey A M, Clark C W and Williams C J 2005 *J. Phys. B: At. Mol. Opt. Phys.* **38** 1687.
- [13] Katori H 2011 *Nat. Photonics* **5** 203.
- [14] Wang Z M, Wu L A, Modugno M, Byrd M S, Yu T *et. al.* 2014 *Phys. Rev. A* **89** 042326.
- [15] Schulte T, Drenkelforth S, Kruse J, Ertmer W, Arlt J *et. al.* 2005 *Phys. Rev. Lett.* **95** 170411.
- [16] Adhikari S K and Salasnich L 2009 *Phys. Rev. A* **80** 023606.
- [17] Nath A and Roy U 2014 *Laser Phys. Lett.* **11** 115501.
- [18] Yamamoto D, Fukuhara T and Danshita I 2020 *Nat. Phys.* **3** 56.
- [19] Billy J, Josse V, Zuo Z, Bernard A, Hambrecht B *et. al.* 2008 *Nature* **453** 891.
- [20] Braun S, Ronzheimer J P, Schreiber M, Hodgman S S, Rom T *et. al.* 2013 *Science* **339** 52.
- [21] Nath A, Bera J, Ghosh S and Roy U 2020 *Sci. Reports* **10** 9016.
- [22] Cheng Y, Gong R and Li H 2006 *Opt. Exp.* **14** 3594.
- [23] Das P, Raju T S, Roy U and Panigrahi P K 2009 *Phys. Rev. A* **79** 015601.
- [24] Nath A, Bera J, Ghosh S, Panigrahi P K, Roy U 2020 *Eur. Phys. J. D* **74** 27.
- [25] Sun Q, Hu J, Wien L, Liu W M, Juzeliunas G *et. al.* 2016 *Sci. Reports* **6** 37679.
- [26] Li J and Zeng J 2021 *Phys. Rev. A* **103** 013320.
- [27] Malomed B A 2006 *Soliton management in periodic systems* (Springer).
- [28] Qiu X, Zou J, Qi X and Li X 2020 *NPJ Quantum Inf.* **6** 87.
- [29] Windpassinger P and Sengstock K 2013 *Rep. Prog. Phys.* **76** 086401.
- [30] Ghosh S, Bera J, Panigrahi P K and Roy U 2019 *Int. J. Quant. Inf.* **17** 1950019.
- [31] Yang B, Sun H, Huang C J, Wang H Y, Deng Y *et. al.* 2020 *Science* **369** 550.
- [32] Bera J, Ghosh S, Salasnich L and Roy U 2020 *Phys. Rev. A* **102** 063323.
- [33] Khaykovich L, Schreck F, Ferrari G, Bourdel T, Cubizolles J *et. al.* 2002 *Science* **296** 1290.
- [34] Inouye S, Andrews M R, Stenger J, Miesner H J, Stamper-Kurn D M *et. al.* 1998 *Nat. Phys.* **392** 151.
- [35] Roberts J L, Claussen N R, Cornish S L and Wieman C E 2000 *Phys. Rev. Lett.* **85** 728.
- [36] Kengne E, Liu W-M, and Malomed B A 2021 *Phys. Rep.* **899** 1-62
- [37] Nath A, and Roy U 2014 *J. Phys. A Math. Theor.* **47** 415301
- [38] Abramowitz M and Stegun I *A Handbook of Mathematical Functions* (1st ed, Dover, New York, NY, USA, 1964).
- [39] Howards L A, Weinhold T J, Shahandeh F, Combes J, Vanner M R, White A G, and Ringbauer M 2019 *Phys. Rev. Lett.* **123** 020402.
- [40] Shukla N, Akhtar N, and Sanders B C 2019 *Phys. Rev. A* **99** 063813.
- [41] Shukla N, Nimmrichter S and Sanders B C 2021 *Phys. Rev. A* **103** 012408.
- [42] Cirac J I, Lewenstein M, Molmer K and Zoller P 1998 *Phys. Rev. A* **57** 1208.
- [43] Zeng B, Zhou D L, Xu Z, Sun C P and You L 2005 *Phys. Rev. A* **71** 022309.
- [44] Foot C J and Shooter M D 2011 *Am. J. Phys.* **79** 762.
- [45] Vo C, Riedl S, Baur S, Rempe G and Durr S 2012 *Phys. Rev. Lett.* **109** 263602.
- [46] Gajdacz M, Opatrny T and Das K K 2014 *Phys. Rev. Lett.* **378** 1919.

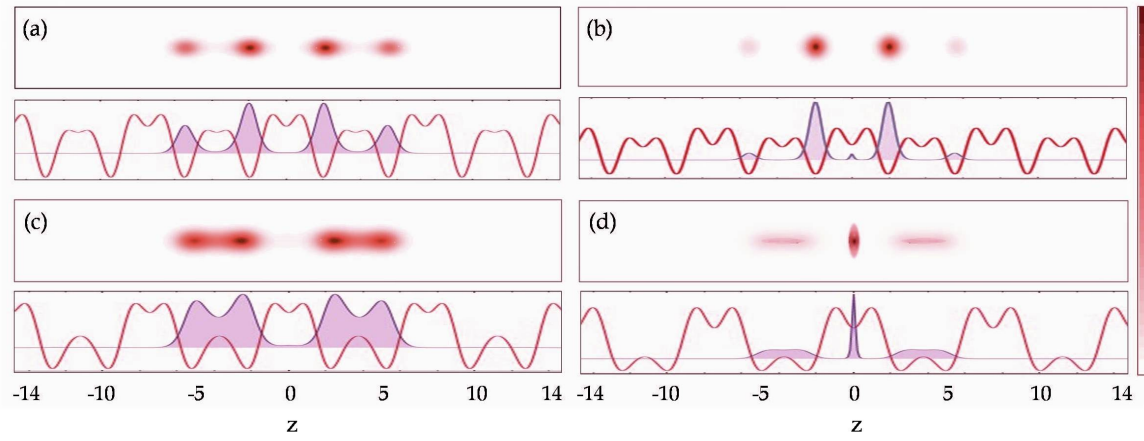


FIG. 3. Condensate density patterns for  $b_1 > 0$  and  $b_2 > 0$ : (a)  $b_1 = 1$ ;  $b_2 = 2$ , (b)  $b_1 = 1$ ;  $b_2 = 3.5$ , (c)  $b_1 = 2$ ;  $b_2 = 1$ , and (d)  $b_1 = 3.5$ ;  $b_2 = 1$ . Each plot of (a)-(d) has two panels: the upper panel shows the contour plot of the density and the lower panel consists of a 2D plot of the density combined with the corresponding potential profile.

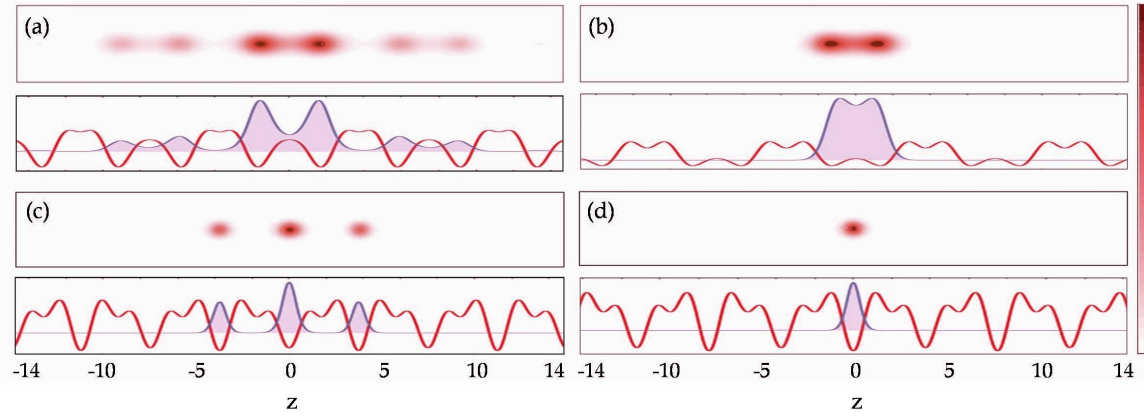


FIG. 4. Condensate density patterns for  $b_1 < 0$  or  $b_2 < 0$  or both: (a)  $b_1 = -1$ ;  $b_2 = 1$ , (b)  $b_1 = -3$ ;  $b_2 = 1$ , (c)  $b_1 = 1$ ;  $b_2 = -3$ , and (d)  $b_1 = -1$ ;  $b_2 = -3$ . Each plot of (a)-(d) has two panels: the upper panel shows the contour plot of the density and the lower panel consists of a 2D plot of the density combined with the corresponding potential profile.

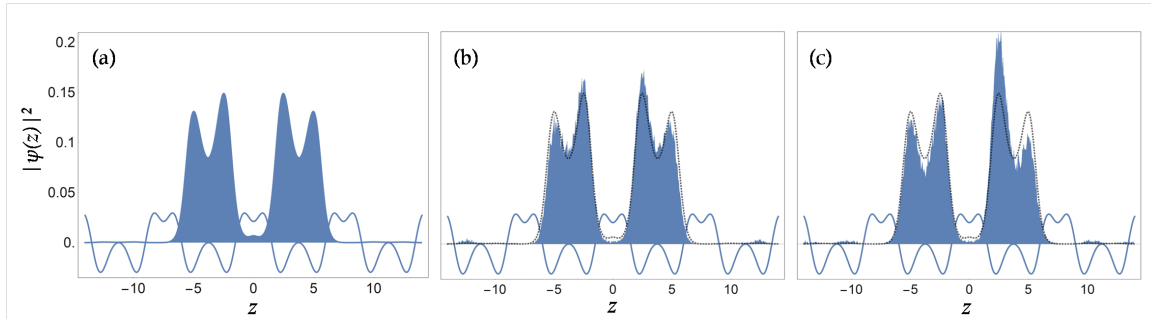


FIG. 5. Condensate densities are depicted by filled plots at times (a)  $t = 0$ , (b)  $t = 10ms$ , and (c)  $t = 20ms$ , along with the potential energy profile (solid-line curve) for  $b_1 = 2$  and  $b_2 = 1$ . Initial density (dotted curve) is merged with the densities in (b-c) for reference.

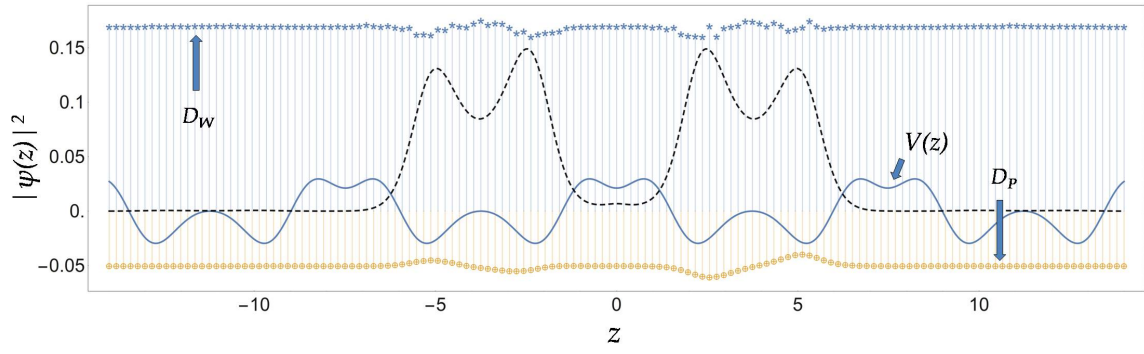


FIG. 6. The numerical stability analysis of one of the obtained solutions with  $b_1 = 2$  and  $b_2 = 1$ . The condensate density is depicted by the dotted line and the trap profile,  $V(z)$  (not in scale), is superimposed on it (the solid line). The deviation of the noisy data from their noise-free counterparts is shown for both kinds of the analyses: the dynamical stability,  $D_W$  (the upper curve, composed of symbols  $*$ ), and the structural stability,  $D_P$  (the lower curve, composed of symbols  $\oplus$ ).